Physics of the Solid State, Vol. 43, No. 10, 2001, pp. 1876–1884. Translated from Fizika Tverdogo Tela, Vol. 43, No. 10, 2001, pp. 1799–1807.

SEMICONDUCTORS AND DIELECTRICS

Polarized ARPES Spectra of Undoped Cuprates

V. A. Gavrichkov*, A. A. Borisov, and S. G. Ovchinnikov

Kirensky Institute of Physics, Siberian Division, Russian Academy of Sciences, Akademgorodok, Krasnoyarsk, 660036 Russia

**e-mail: gav@iph.krasn.ru*

Received January 10, 2001

Abstract—The spectral density (SD) in the ARPES spectra of antiferromagnetic (AFM) dielectrics $Sr_2CuO_2Cl_2$ and $Ca_2CuO_2Cl_2$ along the principal symmetry directions of the Brillouin zone was studied by the generalized tight binding method. At the valence band top of these undoped cuprates in the AFM state, there is a pseudogap of magnetic nature with $E_s(\mathbf{k}) \sim 0$–0.4 eV between a virtual level and the valence band proper. The observed similarity of dispersion along the Γ–M and X–Y directions can be explained by the proximity of the $^3B_{1g}$ triplet and the Zhang–Rice singlet levels. The value of parity of the polarized ARPES spectra at the Γ, M, and X points calculated for the AFM phase of undoped cuprates with an allowance for the partial contributions is even. The conditions favoring observation of the partial contributions in polarized ARPES spectra are indicated. Due to the spin fluctuations, the virtual level acquires dispersion and possesses a small spectral weight. Probably, this level cannot be resolved on the background of the main quasi-particle peak as a result of the damping effects. © *2001 MAIK "Nauka/Interperiodica".*

1. INTRODUCTION

Investigation of dielectrics such as $Sr_2CuO_2Cl_2$ and $Ca_2CuO_2Cl_2$ by the method of angle-resolved photoemission spectroscopy (ARPES) is a means of studying evolution of the electron structure of doped high-temperature superconductors. The available ARPES spectra, measured along the principal symmetry directions for various polarizations of synchrotron radiation, allow the valence states to be classified with respect to the symmetry properties. Indeed, data on the electron structures of both $Sr_2CuO_2Cl_2$ and $Ca_2CuO_2Cl_2$ allow three groups of the valence states to be distinguished, the first group being invariant relative to the reflection from the plane of emission and the second and third groups being even and odd with respect to this reflection. According to the selection rules [1], the ARPES spectra measured with a polarization vector parallel to the plane of emission should show only the even group of states, while the spectra recorded for the perpendicular polarization should display only the odd group. In the perpendicular geometry, the polarization vector is always parallel to the CuO_2 plane. Therefore, contributions due to the p_z and d_z valence states binding the planes into a unified tree-dimensional structure will be observed only in the spectra measured in a parallel geometry.

Let us summarize the main ARPES results [2] related to the problem under consideration:

(i) An analysis of the level occupancies $n(\mathbf{k})$ [3] obtained from the ARPES spectra of antiferromagnetic (AFM) dielectrics $Sr_2CuO_2Cl_2$ and $Ca_2CuO_2Cl_2$ shows the presence of a singularity in $n(\mathbf{k})$ at the intersection with a $\mathbf{k}$ contour (close to the Fermi surface) predicted previously based on the results of band calculations. The quasi-particle peak dispersion on the $\mathbf{k}$ contour of the "remnant Fermi surface" is close to a *d*-like dependence of the $|\cos(k_x a) - \cos(k_y a)|$ type. Since the last function is analogous to a *d*-like dispersion of the pseudogap in undoped $Bi_2Sr_2CaCu_2O_{8+\delta}$(*Dy*)and the superconducting gap in the optimum doped compound, there is an evident relationship between the three energy gap values.

(ii) On the other hand, the $|\cos(k_x a) - \cos(k_y a)|$ relationship has a linear character in the vicinity of the point $M = (\pi/2; \pi/2)$. A similar linear relationship $\sim J\sqrt{\cos^2(k_x a) - \cos^2(k_y a)}$ was observed for the dispersion of spinons [4]. However, the experimental dispersion in the vicinity of M seems to be quadratic rather than linear [2].

(iii) Although the observed dispersion is well described within the framework of the t–t'–t''–J model, there is one special point in application of this model to real systems. According to the t–t'–t''–J model, dispersion along the $\Gamma(0, 0)$–$M(\pi, \pi)$ and $X(\pi, 0)$–$Y(0, \pi)$ directions is related to different parameters (J and t', respectively). Therefore, the observed analogy of the dispersion relationships along these different directions poses inexpediently strict limitations on the model parameters. The existing explanations of the observed universality are related to the self-consistent Born approximation in the t–t'–t''–J model theory [5].

(iv) The results of experiments with polarized radiation are indicative of an even parity of the ARPES spectra of dielectrics in the symmetric points Γ, M, X, and Y [6], the value of the parity being dependent on the doping level. However, parity cannot be interpreted within the framework of the t–t'–t''–J model. For this

reason, theoretical investigations devoted to polarized ARPES spectra usually employ the local density approximation (LDA) in the density functional method (DFM) [7]. The results obtained within the framework of LDA allow the parity to be analyzed. Unfortunately, the dispersion law is not treated as successfully as is the t–t'–t''–J model. In particular, the LDA approach fails to reproduce the quasi-particle peak corresponding to the Zhang–Rice state at the valence band top.

The purpose of this study was to analyze the density of states (SD) spectrum for oxychlorides $Sr_2CuO_2Cl_2$ and $Ca_2CuO_2Cl_2$ based on the ARPES data for various polarizations. The results obtained within the framework of the generalized tight binding method (GTBM) [8] offer a natural generalization of the t–t'–t''–J model and allow clear physical interpretation.

The first section of this paper gives a brief outline of the GTBM and introduces basic formulas for the dispersion and SD. The second section presents the result of numerical calculations of the dispersion relationships and the quasi-particle peak amplitude in the spectral density along the Γ–M–X–Y and X–Y directions in the paramagnetic (PM) and AFM phases. Partial contributions to the SD due to various orbitals are calculated, which is important for identification of ARPES spectra that may differ both in the parity and in scattering cross sections for the incident radiation. The nature of the energy gap is established and the shape of dispersion is determined along the **k** contour of the remnant Fermi surface. The third section gives a symmetry analysis of the partial contributions at the Γ, M, X, and Y points and indicates polarizations for which these contributions can be observed, and the even parity of the total contribution is revealed. The fourth section considers the influence of spin fluctuations on the energy band structure of oxychlorides.

2. SPECTRAL DENSITY OF STATES IN THE GENERALIZED TIGHT-BINDING METHOD

Here, we will briefly formulate the GTBM for a CuO_6 (CuO_4Cl_2) cluster considered as a unit cell. The problem of nonorthogonality of the molecular orbitals of neighboring clusters is explicitly solved by constructing the corresponding Wannier functions on the $d_{x^2-y^2}$, $d_{3z^2-r^2}$, p_x, p_y, p_z five-orbital initial basis set of atomic states.

In the new symmetric basis set, a single-cell part of the Hamiltonian is factorized, making it possible to classify, according to symmetry, all the possible effective single-particle excitations in the CuO_2 plane. Subsequent exact diagonalization of the unit-cell Hamiltonian and the transition to the Hubbard operator representation make it possible to take into account the hopping part of the Hamiltonian.

The initial Hamiltonian of a multiband p–d model can be written in the standard form:

$$
\begin{aligned}
H &= H_d + H_p + H_{pd} + H_{pp}, \quad H_d = \sum_r H_d(r), \\
H_d(r) &= \sum_{\lambda\sigma}\Bigg[(\varepsilon_\lambda - \mu)d^+_{\lambda r\sigma}d_{\lambda r\sigma} + \frac{1}{2}U_\lambda n^\sigma_{\lambda r}n^{-\sigma}_{\lambda r} \\
&+ \sum_{\lambda'\sigma'}\left(-J_d d^+_{\lambda r\sigma}d_{\lambda r\sigma'}d^+_{\lambda' r\sigma'}d_{\lambda' r\sigma} + \sum_{r'}V_{\lambda\lambda'}n^\sigma_{\lambda r}n^{\sigma'}_{\lambda' r'}\right)\Bigg], \\
H_p &= \sum_i H_p(i), \quad H_p(i) = \sum_{\alpha\sigma}\Bigg[(\varepsilon_\alpha - \mu)p^+_{\alpha i\sigma}p_{\alpha i\sigma} \\
&+ \frac{1}{2}U_\alpha n^\sigma_{\alpha i}n^{-\sigma}_{\alpha i} + \sum_{\alpha' i'\sigma'}V_{\alpha\alpha'}n^\sigma_{\alpha i}n^{\sigma'}_{\alpha' i'}\Bigg], \\
H_{pd} &= \sum_{\langle i,r\rangle}H_{pd}(i,r), \\
H_{pd}(i,r) &= \sum_{\alpha\lambda\sigma\sigma'}(t_{\lambda\alpha}p^+_{\alpha i\sigma}d_{r\lambda\sigma} + V_{\alpha\lambda}n^\sigma_{\alpha i}n^{\sigma'}_{\lambda r}), \\
H_{pp} &= \sum_{\langle i,j\rangle}\sum_{\alpha\beta\sigma}(t_{\alpha\beta}p^+_{\alpha i\sigma}p_{\beta j\sigma} + \text{H.c.}),
\end{aligned}
\tag{1}
$$

where $n^\sigma_{\lambda i} = d^+_{\lambda i\sigma}d_{\lambda i\sigma}$ and $n^\sigma_{\alpha i} = p^+_{\alpha i\sigma}p_{\alpha i\sigma}$. Here, the indices r and i run through the positions of $d_{x^2-y^2}$, $d_{3z^2-r^2}$ and p_x, p_y, p_z sets of localized atomic orbitals. Similarly, $\varepsilon_\lambda = \varepsilon_{d_x}$ ($\lambda = d_x$), ε_{d_z} ($\lambda = d_z$) and $\varepsilon_\alpha = \varepsilon_p$ ($\alpha = p_x, p_y$), ε_{p_z} ($\alpha = p_z$) are the energies of the corresponding atomic orbitals; $t_{\lambda\alpha} = t_{pd}$ ($\lambda = d_x$; $\alpha = p_x, p_y$) and $t_{pd}/\sqrt{3}$ ($\lambda = d_z$, $\alpha = p_x, p_y$) are the matrix elements for the copper–oxygen hopping; $t_{\alpha\beta} = t_{pp}$ are the matrix elements of hopping between nearest-neighbor oxygen ions; $U_\lambda = U_d$ ($\lambda = d_x, d_z$) and $U_\alpha = U_p$ ($a = p_x, p_y, p_z$) are the interatomic Coulomb interactions on copper and oxygen atoms, respectively; and $V_{\alpha\lambda} = V_{pd}$ ($\alpha = p_x, p_y$; $\lambda = d_x, d_z$) and V'_{pd} ($\alpha = p_z$; $\lambda = d_x, d_z$) are the copper–oxygen Coulomb repulsion energies. All matrix elements of the Coulomb and exchange interaction are assumed to be independent of the shape of the d or p in-plane orbitals. The primed values refer to the interaction with apical oxygen in CuO_6 or with chlorine in CuO_4Cl_2. Subsequent steps in the conversion of Hamiltonian (1) are analogous to those described in [8]. Here, we will only write the key formulas. All calculations were carried out for the CuO_2 plane divided into CuO_6 (CuO_4Cl_2) clusters.

Using the linear transformation $\hat{S}$, we introduce the new operators $a_{k\sigma}$ and $b_{k\sigma}$ of the hole annihilation in the molecular orbitals of oxygen:

$$\begin{pmatrix} b_{k\sigma} \\ a_{k\sigma} \end{pmatrix} = \hat{S}\begin{pmatrix} p_{xk\sigma} \\ p_{yk\sigma} \end{pmatrix} = \begin{pmatrix} is_x/\mu_k & is_y/\mu_k \\ is_y/\mu_k & -is_x/\mu_k \end{pmatrix}\begin{pmatrix} p_{xk\sigma} \\ p_{yk\sigma} \end{pmatrix}, \quad (2)$$

$$\mu_k^2 = s_x^2 + s_y^2, \quad |\hat{S}| = 1.$$

The new operators satisfy the required commutation relationships $\{b_{k\sigma}^+, a_{p\sigma}\} = 0$. In the new representation, Hamiltonian (1) acquires the form of a sum of intracell (H_c) and intercell (H_{cc}) contributions

$$H = H_c + H_{cc}, \; H_c = \sum_{f\sigma} H_{f\sigma}, \; H_{f\sigma} = h^{(a)} + h^{(b)} + h^{(ab)},$$

$$h^{(b)} = (\varepsilon_b n_b^\sigma + \varepsilon_{d_x} n_{d_x}^\sigma) + \frac{1}{2}U_d n_{d_x}^\sigma n_{d_x}^{-\sigma}$$

$$+ \frac{1}{2}U_b n_b^\sigma n_b^{-\sigma} + \sum_{\sigma'} V_{pd} n_{d_x}^\sigma n_b^{\sigma'} - \tau_b(d_{x\sigma}^+ b_\sigma + \text{H.c.}),$$

$$h^{(a)} = (\varepsilon_a n_a^\sigma + \varepsilon_{d_z} n_{d_z}^\sigma + \varepsilon_{p_z} n_{p_z}^\sigma) + \frac{1}{2}U_d n_{d_z}^\sigma n_{d_z}^{-\sigma} + \frac{1}{2}U_a n_a^\sigma n_a^{-\sigma}$$

$$+ \frac{1}{2}U_p' n_{p_z}^\sigma n_{p_z}^{-\sigma} + \sum_{\sigma'}(V_{pd} n_{d_z}^\sigma n_{p_z}^{\sigma'} + V_{pd} n_{d_z}^\sigma n_a^{\sigma'})$$

$$+ \tau_a(d_{z\sigma}^+ a_\sigma + \text{h.c.}) - \tau_{pd}'(d_{z\sigma}^+ + \text{h.c.}) - t_{pp}'(a_\sigma^+ p_{z\sigma} + \text{h.c.});$$

$$h^{(ab)} = \sum_{\sigma'} U_d n_{d_x}^\sigma n_{d_x}^{\sigma'} + U_{ab} n_a^\sigma n_b^{\sigma'}$$

$$+ V_{pd} n_{d_x}^\sigma n_a^{\sigma'} + V_{pd} n_b^\sigma n_{d_z}^{\sigma'} + V_{pd}' n_{d_x}^\sigma n_{p_z}^{\sigma'}, \quad (3)$$

$$H_{cc} = \sum_{(i \neq j)} \sum_\sigma (h_{\text{hop}}^{(b)} + h_{\text{hop}}^{(a)} + h_{\text{hop}}^{(ab)}),$$

$$h_{\text{hop}}^{(b)} = -2t_{pd}\mu_{ij}(d_{xi\sigma}^+ b_{j\sigma} + b_{i\sigma}^+ d_{xi\sigma}) - 2t_{pp}\nu_{ij} b_{i\sigma}^+ b_{j\sigma},$$

$$h_{\text{hop}}^{(a)} = \frac{2t_{pd}}{\sqrt{3}}\lambda_y(d_{zi\sigma}^+ a_{j\sigma} + \text{H.c.})$$

$$+ 2t_{pp}\nu_{ij} a_{i\sigma}^+ a_{j\sigma} - 2t_{pp}'\lambda_{ij}(p_{zi\sigma}^+ a_{j\sigma} + \text{H.c.}),$$

$$h_{\text{hop}}^{(ab)} = \frac{2t_{pd}}{\sqrt{3}}\xi y(d_{zi\sigma}^+ b_{j\sigma} + \text{H.c.})$$

$$+ 2t_{pp}\chi_{ij}(a_{i\sigma}^+ b_{j\sigma} + \text{h.c.}) - 2t_{pp}'\xi_{ij}(p_{zi\sigma}^+ b_{j\sigma} + \text{H.c.}),$$

where

$$\varepsilon_b = \varepsilon_p - 2t_{pp}\nu_{00}, \quad \varepsilon_a = \varepsilon_p + 2t_{pp}\nu_{00},$$

$$\tau_b = 2t_{pd}\mu_{00}, \quad \tau_a = 2t_{pd}\lambda_{00}/\sqrt{3},$$

$$\tau_{pd}' = 2t_{pd}'/\sqrt{3}, \quad \tau_{pp}' = 2t_{pp}'\lambda_{00}.$$

The coefficients μ_{ij}, ν_{ij}, and λ_{ij} concern to the hybridization of states of the same symmetry and depend only on the distance between the ith and jth cells. The coefficients ξ_{ij} and χ_{ij} concern to the hybridization of states belonging to different a_1 and b_1 representations and change sign upon reflection along either the x and y axis. Expressions for these coefficients are derived in [8, 9].

Now let us determine the eigenvalues and eigenstates of the single-cell Hamiltonian H_c, after which the total Hamiltonian can be rewritten in terms of these eigenstates. In the vacuum sector, the eigenstate is $a^{10}p^6$ or $|0\rangle$. In the single-hole b_1 sector on the basis of $|d_{x\sigma}^+|0\rangle$ and $|b_\sigma^+|0\rangle$ states, the eigenvectors $|\tilde{b}_p\rangle = \beta_p(b)|b_\sigma^+|0\rangle + \beta_p(d_x)|d_{x\sigma}^+|0\rangle$ with the energies $\varepsilon_{1\tilde{b}_p}$ ($p = 1, 2$) can be found through exact diagonalization of the matrix:

$$\hat{h}^{(b)} = \begin{pmatrix} \varepsilon_{d_x} & -\tau_b \\ -\tau_b & \varepsilon_b \end{pmatrix}. \quad (4)$$

In the single-hole a_1 sector on the basis of $|a_\sigma^+|0\rangle$, $|p_{z\sigma}^+|0\rangle$, and $|d_{z\sigma}^+|0\rangle$ states, the eigenvectors $|\tilde{a}_p\rangle = \alpha_p(a)|a_\sigma^+|0\rangle + \alpha_p(p_z)|p_\sigma^+|0\rangle + \alpha_p(d_z)|d_{z\sigma}^+|0\rangle$ with the energies $\varepsilon_{1\tilde{a}_p}$ ($p = 1, 2, 3$) can be found through exact diagonalization of the matrix:

$$\hat{h}^{(a)} = \begin{pmatrix} \varepsilon_{d_z} & \tau_a & -\tau_{pd}' \\ \tau_a & \varepsilon_a & -t_{pd}' \\ -\tau_{pd}' & -t_{pd}' & \varepsilon_{p_z} \end{pmatrix}. \quad (5)$$

By the same way, we determine the eigenstates $|\tilde{A}_q\rangle$ with the energies $\varepsilon_{2\tilde{A}_q}$ in the two-hole A_1 sector $|\tilde{A}_q\rangle = \sum_i A_{qi}|A_i\rangle$, where the coefficients are the eigenvectors A_i (i, q = 1–9), and the basis set of singlet functions $|\tilde{A}_q\rangle$. One of these basis set states represents the Zhang–Rice singlet $|\text{ZR}\rangle$. In the two-hole B_1 sector, we find the triplet eigenvectors $|\tilde{B}_{qM}\rangle = \sum_i B_{qi}|B_{iM}\rangle$ (q = 1– 6; $M = -1, 0, 1$) with the energies $\varepsilon_{2\tilde{B}_q}$, coefficients B_{qi}, and basis set functions $|B_{qM}\rangle$. Thus, diagonalization of the Hamiltonian for a CuO_6 (CuO_4Cl_2) cluster is performed separately in various sectors with the number of holes $n = 0$, 1, or 2.

Previously [10], we found two basic possibilities for stabilizing the $|\tilde{B}_{1M}\rangle$ state as the ground state: (i) with decreasing energy of the p orbitals of O (or Cl) ions in the apical position and (ii) with decreasing crystal-field

parameter $\Delta_d = \varepsilon_{d_z} - \varepsilon_{d_x}$. According to estimates [10], the energy interval between triplet and singlet sates is $\Delta\varepsilon_2 \sim 0.5$ eV. The existence of two states $|\tilde{A}_1\rangle$ and $|\tilde{B}_{1M}\rangle$ with competing energies in the region of realistic values of the parameters implies that both these states have to be taken into account as basis states in our model and that no further reduction to an effective single-band Hubbard model or the *t*–*t*'–*t*"–*J* model is possible. As a result of the exact diagonalization, the Hamiltonian H_c for the AFM phase acquires the following form:

$$H_c = \sum_{pf_G\sigma}(\varepsilon_{1pG} - \mu)X^{pp}_{f_G\sigma} + \sum_{qf_G\sigma}(\varepsilon_{2qG} - 2\mu)X^{qq}_{f_G\sigma}, \qquad f_G = \begin{cases} f_A, & f \in A \\ f_B, & b \in B. \end{cases} \tag{6}$$

Here, *p* and *q* enumerate the single- and two-hole terms of a cell, respectively, and $X^{pq}_f = |p\rangle\langle q|$ are the Hubbard operators constructed on the exact states of the cell. The sublattice levels are split by the field of the AFM state: $\varepsilon_{1pA} = \varepsilon_{1p} - \sigma h$, $\varepsilon_{1pB} = \varepsilon_{1p} + \sigma h$, where the quantity $h \sim J\langle S_z\rangle$ and *J* is the effective exchange interaction between nearest neighbors. As the doping level increases, the *h* value drops to vanish completely in the PM phase. In this paper, the consideration is restricted to a non-self-consistent calculation in which the magnetic state is assumed to be known (AFM or PM at $T = 0$). In the new basis set, the single-electron operators are expressed as

$$c_{f\lambda\sigma} = \sum_m \gamma_{\lambda\sigma}(m)X^m_{f\sigma}, \tag{7}$$

where $c_{\lambda f\sigma} = d_{xf\sigma}, d_{zf\sigma}, a_{f\sigma}, b_{f\sigma}, p_{zf\sigma}$ and *m* is the number of the root vector $\boldsymbol{\alpha}_m(pq)$. To simplify treatment of the Hubbard operators, we use a convenient notation proposed by Zaĭtsev [11]. The matrix elements $\gamma_{\lambda\sigma}(m)$ ($m = 0, 1, \ldots, 31$) corresponding to the above root vectors can be directly calculated upon exact diagonalization of the Hamiltonian H_c; the results of such a calculation are presented in [8]. We take into account only two lower terms: b_1, a_1 in the single-particle sector and $\tilde{A}_1$, $\tilde{B}_{1M}$ in the two-particle sector. This corresponds to $|p\rangle = |\tilde{a}_1\rangle, |\tilde{b}_1\rangle$ and $|q\rangle = |\tilde{A}_1\rangle, |\tilde{B}_{1M}\rangle$ in Eq. (6). All other terms correspond to higher energies and can be ignored as far as the physics of low-energy excitations is considered. The corresponding dispersion relationships for the valence band were derived using equations of motion for Green's functions constructed on Hubbard operators:

$$C^{\lambda\lambda'}_{k\sigma} = \langle\langle c_{k\lambda\sigma}|c^+_{k\lambda'\sigma}\rangle\rangle_E = \sum_{mn}\gamma_{\lambda\sigma}(m)\gamma^+_{\lambda'\sigma}(n)D^{mn}_{k\sigma}, \tag{8}$$

where

$$\hat{D}_{k\sigma} = \begin{pmatrix} \hat{D}_{k\sigma}(AA) & \hat{D}_{k\sigma}(AB) \\ \hat{D}_{k\sigma}(BA) & \hat{D}_{k\sigma}(BB) \end{pmatrix},$$

$$D^{mn}_{k\sigma}(AB) = \langle\langle X^m_{k\sigma}|Y^n_{k\sigma}\rangle\rangle_E.$$

In the Hubbard I approximation, the dispersion relationship is determined by the equation

$$\left\| (E - \Omega^G_m)\delta_{mn}/F^G_\sigma(m) - 2\sum_{\lambda\lambda'}\gamma^*_{\lambda\sigma}(m)T^{PG}_{\lambda\lambda'}(\mathbf{k})\gamma_{\lambda'\sigma}(n) \right\| = 0. \tag{9}$$

This relationship is similar to the standard single-electron equation for the tight-binding method but differs from the latter in two respects. First, the single-particle energies are determined as resonances between multielectron states. Second, the occupation factors $F^G_\sigma(m) = \langle X^{pq}_{f_G\sigma}\rangle + \langle X^{qq}_{f_G\sigma}\rangle$ lead to a concentration dependence of both the dispersion relationships and the quasi-particle peak amplitude in the SD. Mathematically, we deal with an equation of the generalized eigenvalue problem, with the matrix of the inverse occupation factors replacing the ordinary "nonorthogonality matrix." Each root vector $\boldsymbol{\alpha}_m$ determines a charged Fermi quasi-particle with spin 1/2 and local energy $\Omega^G_m = \varepsilon_{2qG} - \varepsilon_{1pG}$.

Equation (9) is a convenient means of calculating the dispersion relationships, which allows all possible quasi-particle states to be determined. However, not all of these theoretically possible sates can be observed in experiment. As is known, the ARPES measurements give the amplitude of the quasi-particle peaks in SD

$$A_\sigma(\mathbf{k}, E) = \left(-\frac{1}{\pi}\right)\sum_\lambda \mathrm{Im}(G^{\lambda\lambda}_{k\sigma}) = \left(-\frac{1}{\pi}\right)\sum_{\lambda mn}\gamma_{\lambda\sigma}(m) \times \gamma^+_{\lambda\sigma}(n)\mathrm{Im}(D^{mn}_{k\sigma}(AA) + D^{mn}_{k\sigma}(BB)), \tag{10}$$

rather than a dispersion law as such. Owing to the corresponding occupation factors, the SD may become negligibly small or even vanish for some quasi-particles. As a result, the corresponding peak will be missing from the spectrum. The high dimensionality of the $\hat{D}_{k\sigma}$ matrix (32×32) makes analytical representation of SD impossible. We have performed a numerical calculation of the SD using relationship (10) for the principal symmetry directions of the Brillouin zone at $T = 0$. For the PM phase, the dispersion law and the SD can be obtained using single- sublattice analogs of Eqs. (9) and (10).

3. NUMERICAL CALCULATION OF SPECTRAL DENSITY

Figure 1 shows the results of the numerical calculation of dispersion along the principal symmetry directions of the Brillouin zone for a quasi-particle peak at the valence band top of $Sr_2CuO_2Cl_2$ and $Ca_2CuO_2Cl_2$ compounds in the AFM and PM states at $T = 0$. In the PM phase, the calculated dispersion law is analogous to that observed in optimum doped samples of $Bi_2Sr_2CaCu_2O_{8+\delta}(Dy)$ [12]. The most interesting feature of our theoretical spectrum is the presence of an energy level with a zero SD at the very top of the valence band, which is not manifested in the experimental ARPES spectra. Indeed, the undoped AFM sample contains only $\boldsymbol{\alpha}_{0\sigma}(\tilde{b}_{1\uparrow} - \tilde{A}_1)$ and $\boldsymbol{\alpha}_{0\sigma}(\tilde{b}_{1\downarrow} - \tilde{A}_1)$ quasi-particles at the valence band top. At zero temperature, with neglect of the quantum fluctuations, the filling numbers for a single-hole $|\tilde{b}_{1\sigma}\rangle$ state in one of the spin projections are zero for both *A* and *B* sublattices. Therefore, one of the spin projections in the undoped compound possesses a nondispersive level called the virtual level [8]. Since the transitions between empty states have zero amplitude, a peak corresponding to transitions involving this level is not observed in the SD. This is a typical manifestation of the strong correlation effect.

Thus, the energy gap between the valence and conduction band in oxychlorides at $T = 0$ can be represented as $E_g(\mathbf{k}) = E_{ct}(\mathbf{k}) + E_S(\mathbf{k})$, where $E_{ct}(\mathbf{k})$ is the charge transfer gap and $E_S(\mathbf{k})$ is the gap between the virtual level and the valence band. Since both these terms refer to quasi-particles of the same type (with the same spin projection) existing on the background of different components of the spin doublet $|b_\sigma\rangle$, the gap $E_S(\mathbf{k})$ has a magnetic nature and is absent in the PM phase. Taking into account the absence of the main characteristic signs of the semiconductor gap and the zero value at $\mathbf{k} = M$, the $E_S(\mathbf{k})$ value will be referred to as the pseudogap.

Figure 2 presents the dispersion of the pseudogap $E_S(\mathbf{k})$ along the boundary of the AFM Brillouin zone on the background of the *d*-like dependence of the $|\cos(k_x a) - \cos(k_y a)|$ type. This diagram demonstrates a clear relationship between the pseudogap in AFM dielectrics, the pseudogap in weakly doped compounds, and the superconducting gap in optimum doped samples [2]. Proximity of the calculated law to the experimentally observed dispersion [2] suggests that the **k** contour of the remnant Fermi surface observed by Ronning *et al.* [3] in AFM dielectric $Ca_2CuO_2Cl_2$ can be an ARPES signal from the valence band. A possible reason for this is the purely two-dimensional character of the quasi-particle states on any **k** contour close to the $X \rightleftharpoons Y$ contour. In all other symmetry directions, the calculation reproduces nonzero contributions to SD from the out-of-plane d_z and p_z molecular orbitals (see below). The factors $T_{\lambda\lambda'}(k) = \frac{1}{N}\sum_{R_i} T_{\lambda\lambda'}(\mathbf{R}_i) e^{ikR_i}$ in Eq. (9) contain no inter-sublattice terms for any **k** on the $X \rightleftharpoons Y$ contour, so that the dispersion along this contour can be only of the $\sim\cos(k_x a)\cos(k_y a)$ type. As expected, this dispersion curve precisely fits the results of our numerical calculation (Fig. 2). The experiment more likely corresponds to a linear dispersion in the vicinity of the point *M* [2] and we believe that it is not $|\cos(k_x a) - \cos(k_y a)|$, but it is $\cos(k_x a)\cos(k_y a)$ relationship.

According to the results of our calculations, a reason for the similar dispersion patterns observed in the AFM phase along the Γ–*M* and *X*–*Y* symmetry directions is a

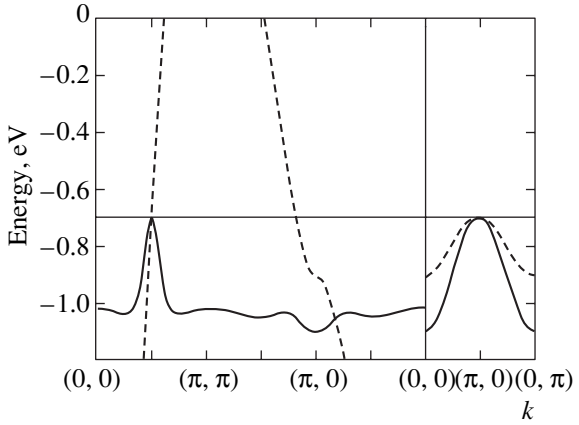

Fig. 1. Dispersion at the valence band top along the main symmetry directions of the Brillouin zone of the AFM (solid curve) and PM (dashed curve) phases at $T = 0$ calculated by Eq. (9).

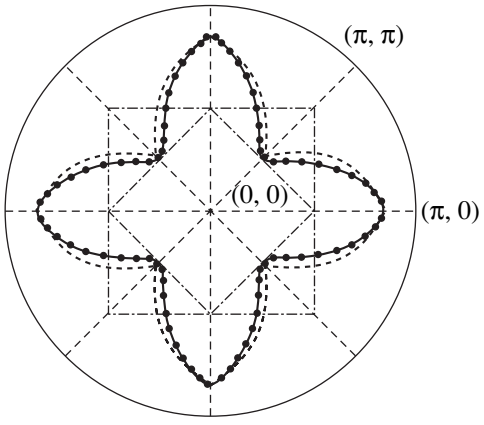

Fig. 2. Dispersion of the $E_S(\mathbf{k})$ pseudogap along the $X \rightleftharpoons Y$ contour, representing $|\cos(k_x a) - \cos(k_y a)|$ (dashed curve), $|\cos(k_x a)\cos(k_y a)|$ (solid curve), and numerical calculations by formula (9) (points). The dispersion is given by the distance from the AFM Brillouin zone boundary to the point of calculation.

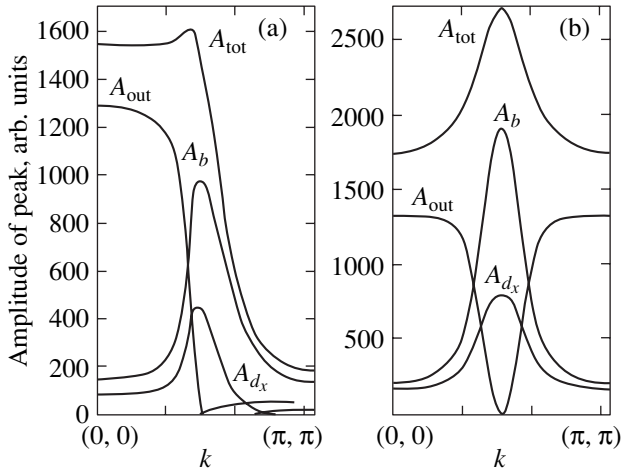

Fig. 3. **k**-Dependences of the partial contributions to the quasi- particle peak amplitude along the Γ–*M* direction for (a) PM and (b) AFM phases.

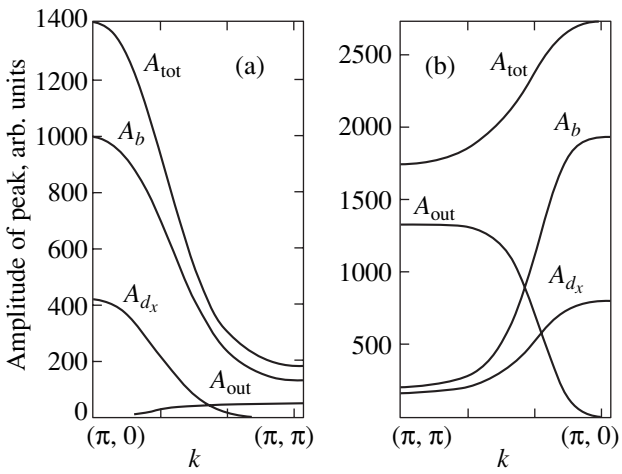

Fig. 4. **k**-Dependences of the partial contributions to the quasi- particle peak amplitude along the *M*–*X* direction for (a) PM and (b) AFM phases.

strong hybridization of the valence band of the Zhang–Rice singlet and the lower band of the $^3B_{1g}$ triplet at the points Γ and *M*. According to our data, the observed similarity is determined only by the values of parameters related to apical Cl or O ions. In addition, our results reveal a strong anisotropy of the effective mass in the vicinity of $\mathbf{k} = M$ ($m_{\text{eff}}^{XY}/m_{\text{eff}}^{\Gamma M} \sim 10$). Therefore, the similarity refers only to the dispersion width in these directions.

The SD $A(\mathbf{k}, E)$ was calculated along the four principal symmetry directions of the Brillouin zone: Γ–*M*, *M*–*X*, *X*–Γ, and *X*–*Y* for PM and AFM phases. According to Eq. (10), the SD is additive. Therefore, we may determine the partial SD contributions due to all orbitals involved in the calculation:

$$A(\mathbf{k}, E) = \sum_{\lambda\sigma} A_{\lambda\sigma}(\mathbf{k}, E),$$

where $\lambda = d_x$, *b*, *a*, d_z, and p_z. As will be demonstrated below, the additive representation offers a convenient approach to analysis of the polarized ARPES spectra.

Figures 3a and 3b show **k**-dependences of the SD amplitude and the partial contributions along the Γ–*M* symmetry direction for AFM and PM phases, respectively. For realistic values of the parameters used in the calculation [8], the $^3B_{1g}$ triplet level is 0.7 eV higher than the A_{1g} level of the Zhang–Rice singlet. As expected, the **k**-profile of the quasi-particle peak amplitude loses symmetry relative to the point *M* upon transition to the PM phase. If the contribution due to the out-of-plane orbitals $A_{\text{out}}(\mathbf{k}, E) = A_{d_z}(\mathbf{k}, E) + A_{p_z}(\mathbf{k}, E)$ is still dominant at $\mathbf{k} = \Gamma$, the quasi-particle peak amplitude at the point *M* significantly decreases. The residual SD at this symmetry point is due to the admixture of states from the conduction band involving only in-plane d_x and *b* orbitals.

Figures 4a and 4b show the **k**-dependences of the quasi-particle peak amplitude along the *M*–*X* symmetry direction of the Brillouin zone. In both AFM and PM phases, only the in-plane *b* and d_x orbitals $A_{\text{pl}}(\mathbf{k}, E) = A_{d_x}(\mathbf{k}, E) + A_b(\mathbf{k}, E)$ contribute at the point $\mathbf{k} = X$, while the contributions from p_z and d_z states at this symmetry point vanish. The total amplitude of SD monotonically increases along the *M*–*X* direction in both AFM and PM phases. Of special interest was the symmetry direction Γ–*X* (Figs. 5a, 5b). Here, in addition to the analogous suppression of the partial contribution $A_{\text{out}}(\mathbf{k}, E)$ at the point $\mathbf{k} = X$, there is a crossover from monotonic growth

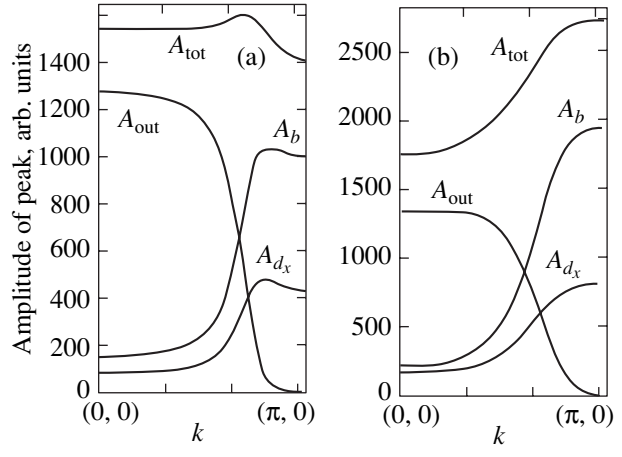

Fig. 5. **k**-Dependences of the partial contributions to the quasi- particle peak amplitude along the Γ–*X* direction for (a) PM and (b) AFM phases.

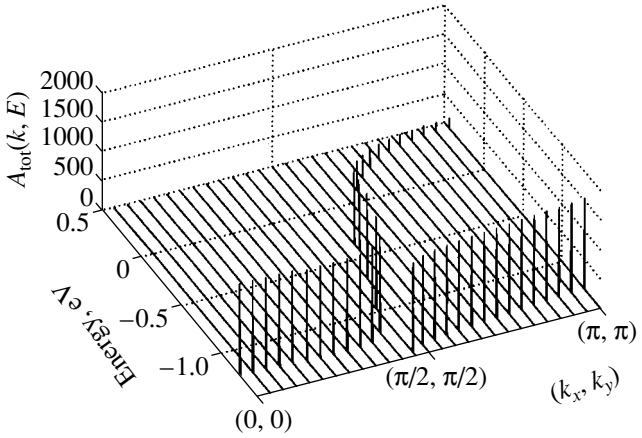

Fig. 6. Three-dimensional **k**-dependences of the amplitude of the quasi-particle peak along the Γ–*M* direction for the PM phase.

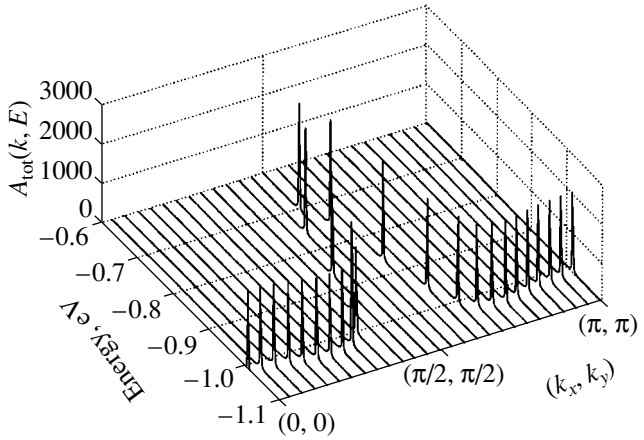

Fig. 7. Three-dimensional **k**-dependences of the amplitude of the quasi-particle peak along the Γ–*M* direction for the AFM phase.

in the quasi-particle peak amplitude in the AFM phase to nonmonotonic behavior with a maximum at **k** = $(2\pi/3, 0)$ in the PM phase. An analogous maximum was observed in the ARPES spectra of $Ca_2CuO_2Cl_2$ at T = 150 K [2]. An analysis of the eigenstates in this symmetry direction showed that a maximum at the point ~$(2\pi/3, 0)$ in the PM phase is related to a maximum admixture of the states from the conduction band. The same factor accounts for a maximum in the partial contributions of the in-plane b and d_x orbitals. Along the *X*–*Y* symmetry direction, the quasi-particle peak amplitude containing only the $A_{d_x}(\mathbf{k}, E)$ and $A_b(\mathbf{k}, E)$ contributions is virtually independent of the wavevector.

Figures 6 and 7 show three-dimensional view of $A(\mathbf{k}, E)$ along the Γ–*M* direction. The spectra of both PM and AFM phases exhibit no quasi-particle peak in the region of virtual level energies. The spectrum of the PM phase shows evidence of a triplet contribution to the quasi-particle peak amplitude.

4. POLARIZATION DEPENDENCE OF THE ARPES SPECTRA

Additional information on the nature of states in the valence band can be obtained by comparing ARPES spectra measured using parallel and perpendicular polarizations of the electric vector relative to the photoemission plane.

Let us analyze the polarization dependence of the SD (10) with allowance for parity and the magnitude of the partial contributions. The ARPES spectra will be considered with neglect of the magnetic scattering effects, which are small compared to the charge scattering effects as reflected by the factor $(\hbar\omega/mc^2)$. However, the charge effects are significantly influenced by the presence and type of magnetic ordering.

Data summarized in the table show the **k** groups, irreducible representations, and parities of the in-plane and out-of-plane orbital contributions to the total SD in the Γ, *X*, and *M* symmetry points of the Brillouin zone for the AFM phase. As is seen from these data, the presence of a nonzero photocurrent at the point Γ is related to a small E_u irreducible representation of the **k** group for $\alpha_{0\sigma}(\tilde{b}_{1,\sigma'}\tilde{A}_1^{-1})$ quasi-particles rather than to an additional (satellite) quasi-particle state. A special feature of the photocurrent observe-d at the center of the Brillouin zone is that this signal is proportional only to the SD contribution from oxygen orbitals. The parity of the total SD $A_{tot}(\mathbf{k}, E)$ is indicated with allowance for the partial contributions at the corresponding points of the Brillouin zone.

The states of different parity in the valence band can be probed separately by changing the sample orientation during the ARPES measurements in combination with the linearly polarized radiation. Moreover, it is even possible to observe evolution of the parity with variation of the doping level [6]. In the SD of oxychlorides, a quasi-particle peak was observed in the Γ–*M* and Γ–*X* directions only for the parallel experimental geometry. This is possible only provided that the valence states are even. A simple comparison with the results of polarized ARPES measurements [6] shows that the calculated parity agrees with that observed for the undoped compounds. Since the even parity at the points Γ and *M* is due to the out-of-plane contribution $A_{out}(\mathbf{k}, E)$, the quasi-particle peak amplitude must also depend on the angle of incidence of a radiation polarized in the parallel direction.

5. EFFECT OF SPIN FLUCTUATIONS ON THE BAND STRUCTURE OF ANTIFERROMAGNETS

In our non-self-consistent approach, dependence of the electron structure on the magnetic ordering is mediated by the occupation factors $F_\sigma(m)$ entering into Eq. (9). At

The characteristics of partial contributions to the total SD amplitude in polarized ARPES

	I	II	III	IV
	$\Gamma(D_{4h})$–$M(D_{4h})$		Γ–$X(D_{2h})$	
A_{d_x}	Odd (B_{1g})	Odd (B_{1g})	Even	Even (A_g)
A_b	0 (E_u)	Odd (B_{1g})	0	Even (A_g)
$A_{\text{in}} = A_{d_x} + A_b$	0 + Odd	Odd	0 + Even	Even
A_a	0 (E_u)	Even (A_{1g})	0	Odd (B_{2u})
$A_{\text{out}} = A_{d_z} + A_{p_z} + A_a$	~Even (A_{1g})	Even (A_{1g})	~Even	~Even (A_g)
$A_{\text{tot}} = A_{\text{in}} + A_{\text{out}}$	~Even	~Even	~Even	~Even

Note: Experimental observation conditions: (columns I and III) A_{d_x}, A_b, and A_{out} are observed using perpendicular, arbitrary, and parallel polarization, respectively; (column II) A_{in} and A_{out} are observed using perpendicular and parallel polarization, respectively; (column IV) A_{in} and A_{out} are observed using parallel polarization.

a valence band top, the determining role belongs to the quasi-particles $\boldsymbol{\alpha}_{0\sigma}(\tilde{b}_{1,\sigma'} - {}^1\tilde{A}_1)$, $\boldsymbol{\alpha}_{1\sigma}(\tilde{b}_{1,\sigma'} - {}^3\tilde{B}_{1,0})$, and $\boldsymbol{\alpha}_{2\sigma}(\tilde{b}_{1,\sigma'} - {}^3\tilde{B}_{1,2\sigma})$; in the case of undoped oxychlorides featuring unoccupied two-hole terms, $F_{\sigma'}(\boldsymbol{\alpha}_{1\sigma}) = \langle n_{\tilde{b},\sigma'}\rangle$. For nonzero matrix elements $\gamma_{\lambda\sigma}(m)$ (m = 0, 1, …, 31) given by (7), the occupation factors in the AFM phase with sublattices A: $\langle S_A^z\rangle = \langle S^z\rangle$ and B: $\langle S_B^z\rangle = -\langle S^z\rangle$ can be written in the following form ($\sigma = \pm 1/2$): $F^G_{-\sigma}(\boldsymbol{\alpha}_{0\sigma}) = F^G_{-\sigma}(\boldsymbol{\alpha}_{1\sigma}) = 1/2 - 2\sigma\langle S_G^z\rangle$, $F^G_{\sigma}(\boldsymbol{\alpha}_{2\sigma}) = 1/2 + 2\sigma\langle S_G^z\rangle$ (where $G = A, B$). To the present moment we restricted the consideration to the Ising order, assuming that $\langle S^z\rangle = 1/2$. The simplest way to provide for a self- consistent calculation is to construct an effective Hamiltonian in the form of a Heisenberg Hamiltonian with an antiferromagnetic exchange term J, followed by a self-consistent calculation of $\langle S^z\rangle$. Thus, we may take into account the local spin fluctuations (zero-point fluctuations in the AFM phase), while allowance for the nonlocal fluctuations of the $\langle S_i^+ S_j^-\rangle$ type would require going beyond the scope of the Hubbard I approximation adopted in this study. A detailed analysis of the applicability of such methods and comparison with the available results on the magnetic polarons in the t–t'–J model were made in [13].

As is known, the presence of the zero-point fluctuations gives rise to quantum spin reduction: $\langle S^z\rangle = 1/2 - n_0$, where the n_0 value can be calculated by different methods. According to the spin wave theory, two-dimensional antiferromagnets are characterized by $n_0 \approx 0.2$ [14]. Allowance for the spin fluctuations significantly modifies the energy band structure (Fig. 8). Indeed, the nondispersed level in Fig. 1 has a zero dispersion and a zero spectral weight because $F^A_{\downarrow}(\boldsymbol{\alpha}_{0\uparrow}) = 0$ in the Ising calculation variant. Owing to the spin fluctuations, the occupation factors are $F^A_{\downarrow}(\boldsymbol{\alpha}_{0\uparrow}) = n_0$ and $F^B_{\downarrow}(\boldsymbol{\alpha}_{0\uparrow}) = 1 - n_0$, which yields a nonzero dispersion and a spectral weight ~n_0. Thus, in the presence of spin fluctuations, the band structure of an undoped antiferromagnet is similar to the band structure of a doped Ising ferromagnet with a hole concentration of $x = n_0$. Because of the small spectral weight of the corresponding band, this band appears as a low-energy satellite in the ARPES spectrum. It is not excluded that the damping effects exclude the possibility of resolving this peak. Nevertheless, such satellites, the intensity of which (as well as of the spin fluctuations) increases with the temperature T,

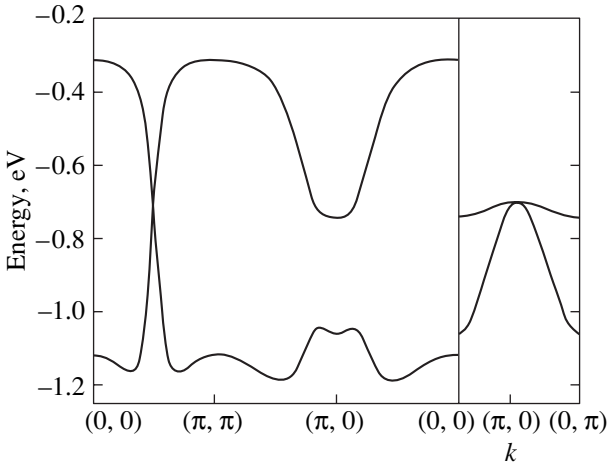

Fig. 8. Dispersion at the valence band top along the main symmetry directions of the Brillouin zone of the AFM phase calculated with an allowance for the spin fluctuations (quantum spin reduction $n_0 = 0.1$).

were recently obtained in calculations performed by the quantum Monte Carlo method within the framework of the Hubbard model [15].

6. CONCLUSIONS

To summarize the results of our calculations, subsequent analysis, and comparison with experimental ARPES data, we point out the following.

(i) Owing to a small energy gap (~0.7 eV) between the $^3B_{1g}$ triplet level and the Zhang–Rice singlet level, a strong hybridization of the singlet valence band and the lower $^3B_{1g}$ triplet band takes place at the Γ and *M* symmetry points. This hybridization accounts for the like patterns of dispersion observed in the Γ–*M* and *X*–*Y* directions of the AFM phase. However, our calculations predict anisotropy of the effective mass at $\mathbf{k} = M$ with a ratio of $m_{\text{eff}}^{XY}/m_{\text{eff}}^{\Gamma M} \approx 10$. On the whole, the valence band does not possess a two-dimensional character. As a result, when the angle of incidence of radiation polarized parallel to the plane of emission deviates from normal, the amplitude of the quasi-particle peak at the Γ and *M* symmetry points in the AFM phase will increase.

(ii) At the valence band top of $Sr_2CuO_2Cl_2$ and $Ca_2CuO_2Cl_2$ in the AFM state, there is a pseudogap of magnetic nature with $E_s(\mathbf{k}) \sim 0$–0.4 eV between a virtual level and the valence band proper; the gap vanishes at the point *M* of the Brillouin zone. The virtual level corresponds to a small SD at $T = 0$, which is proportional to the zero-point spin fluctuation density n_0. Dispersion of the pseudogap in the *X*–*Y* direction agrees well with that on the **k** contour of the remnant Fermi surface. Contribution to the SD in this direction is entirely due to the in-plane d_x and *b* orbitals and, hence, the spectrum has essentially a two-dimensional character. In the PM phase, the pseudogap is absent and the valence band dispersion is analogous to that of $Bi_2Sr_2CaCu_2O_{8+\delta}$(*Dy*) doped to the optimum level [12].

(iii) The parity calculated for the ARPES spectra at the points Γ, *M*, and *X* of the AFM phase with allowance for the partial contributions is even, in agreement with [6]. The presence of a nonzero photocurrent at Γ is related to a small E_u irreducible representation for the $\boldsymbol{\alpha}_{0\sigma}(\tilde{b}_{1,\sigma'} - {}^1\tilde{A}_1)$ quasi-particle state with $\mathbf{k} = \Gamma$ rather than to an additional satellite state. A special feature of the photocurrent observed at the center of the Brillouin zone is that this signal is proportional only to the SD contribution from in-plane oxygen orbitals.

(iv) Allowance for the spin fluctuations significantly modifies the energy band structure. Indeed, the nondispersed level in the AFM phase has a zero dispersion and a zero spectral weight in the Ising calculation scheme. Owing to the spin fluctuations, the level acquires nonzero dispersion and spectral weight. Thus, in the presence of spin fluctuations, the band structure of oxychlorides is similar to the band structure of a doped Ising ferromagnet. Owing to the small spectral weight acquired by the virtual level due to the spin fluctuations, this band appears as a low-energy satellite in the ARPES spectrum. It is not excluded that the damping effects exclude the possibility of observing this peak against the background of the main quasiparticle peak.

ACKNOWLEDGMENTS

The authors are grateful to Prof. A. Lichtehshtein (Holland) for helpful advice, Prof. D.M. Edwards (Great Britain) and Prof. A. Oles (Poland) for their interest in this work, and Prof. W. Nolting (Germany) and his students, T. Hickel and P. Sinyukov, for fruitful discussions.

This study was supported by the Krasnoyarsk Scientific Foundation, project no. 9F0039.

REFERENCES

1. Z. Zangvill, *Physics at Surfaces* (Cambridge Univ. Press, Cambridge, 1988).
2. T. Tohyama and S. Maekawa, Supercond. Sci. Technol. **13**, 17 (2000).
3. F. Ronning, C. Kim, D. I. Feng, *et al.*, Science **282**, 2067 (1998).
4. R. B. Laughlin, Phys. Rev. Lett. **79** (9), 1726 (1997).
5. T. Tohyama, Y. Shibata, S. Maekawa, *et al.*, J. Phys. Soc. Jpn. **69** (9), 3716 (2000).
6. M. Grioni, H. Berger, S. Larosa, *et al.*, Physica B (Amsterdam) **230–232,** 825 (1997).
7. R. Hayn, H. Rosner, V. Yu. Yushankhai, *et al.*, Phys. Rev. B **60** (1), 645 (1999).
8. V. A. Gavrichkov, S. G. Ovchinnikov, A. A. Borisov, and E. G. Goryachev, Zh. Éksp. Teor. Fiz. **118** (2), 422 (2000) [JETP **91**, 369 (2000)].
9. R. Raimondi, J. H. Jefferson, and L. F. Feiner, Phys. Rev. B **53** (13), 8774 (1996).
10. V. A. Gavrichkov and S. G. Ovchinnikov, Fiz. Tverd. Tela (St. Petersburg) **40** (2), 184 (1998) [Phys. Solid State **40**, 163 (1998)].
11. R. O. Zaytsev, Zh. Éksp. Teor. Fiz. **68** (1), 207 (1975) [Sov. Phys. JETP **41**, 100 (1975)].
12. D. S. Marshall, D. S. Dessau, A. G. Loeser, *et al.*, Phys. Rev. Lett. **76** (25), 4841 (1996).
13. S. G. Ovchinnikov, Zh. Éksp. Teor. Fiz. **107** (3), 796 (1995) [JETP **80**, 451 (1995)].
14. P. Horsch and W. von der Linden, Z. Phys. B **72**, 181 (1988).
15. C. Grober, R. Eder, and W. Hanke, Phys. Rev. B **62** (7), 4336 (2000).

Translated by P. Pozdeev